

International Journal of Modern Physics D  
 © World Scientific Publishing Company

## Evidence of variation of the accretion flow geometry in GRS 1915+105 from IXAE and RXTE data

Partha Sarathi Pal<sup>1</sup>, Sandip K. Chakrabarti<sup>2,1</sup> and Anuj Nandi<sup>1,3</sup>

1. Indian Centre for Space Physics, Chalantika 43, Garia Station Rd. Kolkata 700084

2. S.N. Bose National Centre for Basic Sciences, JD Block, Kolkata 700098;  
 chakraba@bose.res.in

3. Space Science Division, ISRO-HQ, New BEL Rd, Bangalore, 560231

The Galactic microquasar GRS 1915+105 exhibits various types of light curves. There is, however, no understanding of when a certain type of light curve will be exhibited and only in a handful of cases, the transitions from one type to another have actually been observed. We study the detailed spectral properties in these cases to show that different classes have different ratio of the power-law photon and the blackbody photon. Since the power-law photons are from the Compton cloud, and the intensity of the power-law photon component depends on the degree of interception of the soft photons by the Compton cloud, we conclude that not only the accretion rate, but the accretion flow geometry must also change during a class transition.

*Keywords:* Black hole Physics – hydrodynamics – accretion, accretion disks – radiative transfer

### 1. Introduction

Indian X-ray Astronomy Experiments (IXAE) payload on board IRS-P3 satellite data of the enigmatic stellar mass black hole binary GRS 1915+105 (Harlaftis & Greiner, 2004) clearly indicated that GRS 1915+105 can have various types of light curves (Yadav et al., 1999; Rao, Yadav & Paul, 2000; Chakrabarti & Nandi, 2000 and references therein; Naik et al. 2002a). So far, a total of thirteen types of light curves have been detected. However, there are only a handful of cases when an actual transition from one type to another has been reported (Chakrabarti et al., 2004; Chakrabarti et al. 2005, hereafter Paper I and Paper II respectively), and those too using the IXAE data which had only two energy channels. It was possible to see the transitions because the IXAE payload observed the same object, namely, GRS 1915+105, for several orbits. Specifically, Papers I and II showed that in a matter of two to three hours indicating that it is not the viscous time scale of the Keplerian disk, but the free-fall time scale of the low-angular momentum halo which decides the variability class transition.

In the present paper, we study the spectra of the classes which showed the transitions and found that one of the parameters which could be responsible for the class transition is the geometry of the Compton cloud. There are various models

2 Partha Sarathi Pal, Sandip K. Chakrabarti, Anuj Nandi

of this cloud, including a Keplerian disk with corona (Haardt & Maraschi, 1993) and the unstable inner edge of the standard disk (Kobayashi et al. 2003). However, we shall use a physically reasonable solution of the two component advective flow (TCAF) model (Chakrabarti & Titarchuk, 1995, hereafter CT95), where, the Compton cloud is made up of the post-shock region of the sub-Keplerian component which includes the jet and the outflows as well. In the literature many works are present which discusses the quasi-periodic oscillations of black hole candidates (e.g., Strohmayer, 2001; Wagoner, Silbergleit, Ortega-Rodriguez, 2001; Stella & Vietri, 1999; Abramowicz, Kluzniak, 2001; Stuchlik, Slan, Trk, 2007; Kato, 2008; Blaes, Sramkova, Abramowicz, Kluzniak & Torkelson, 2007). However, we shall concentrate only on the spectral properties of GRS 1915+105 in the current paper.

The plan of this *letter* is the following: we briefly present the data analysis procedure in our next section. In §3, we study the nature of the components of the spectra, especially the black body and the power-law components. We compute the efficiency of Comptonization by taking the ratio of the photon numbers in those components. We show that indeed, the average ratio varies from class to class. Finally, in §4, we discuss the physics behind such changes in relation to the accretion flow dynamics.

## 2. Observation & Spectral Analysis

In Papers I and II we have already presented the IXAE data analysis procedure. Due to poor spectral and temporal resolutions of IXAE, we take resort to the RXTE science data, which are taken from the NASA HEASARC data archive for analysis. We chose the data procured in 1996-97 by RXTE as in this period GRS 1915+105 has shown almost all types of variabilities in X-rays. We however exclude the data collected for elevation angles less than  $10^\circ$ , offset greater than  $0.02^\circ$  and during the South Atlantic Anomaly (SAA) passage. Since among the four PCUs only PCU1 and PCU2 were working most efficiently and are continuously ON through the observations, we took the data from PCU1 and PCU2 with all the layers in our analysis. In Table. 1, the ObsIDs are given.

Spectral analysis for the PCA data is done by using “standard2” mode data which have 16 sec time resolution. The source spectrum is generated using FTOOLS task “SAEXTRACT” with 16 sec time bin from “standard2” data. The background fits file is generated from the “standard2” fits file by the FTOOLS task “runpcabackest” with the standard FILTER file provided with the package. The background source spectrum is generated using FTOOLS task “SAEXTRACT” with 16 sec time bin from background fits file. The standard FTOOLS task “pcarsp” is used to generate the response file with appropriate detector information. The spectral analysis and modeling was performed using XSPEC (V.12) astrophysical fitting package. For the model fitting of PCA spectra, we have used a systematic error of 1%. The spectra are fitted with *diskbb* and *power-law* model along with  $6.0 \times 10^{22} \text{cm}^{-2}$  hydrogen column absorption (Muno et al., 1999) and we used the

Obs-Id	Class	Date
20402-01-35-00*	$\kappa$	07-07-1997
20402-01-33-00	$\kappa$	18-06-1997
20402-01-31-00*	$\rho$	03-06-1997
20402-01-03-00	$\rho$	19-11-1996
20187-02-01-00*	$\alpha$	07-05-1997
20402-01-30-01	$\alpha$	28-05-1997
10408-01-15-00*	$\theta$	16-06-1996
20402-01-45-02	$\theta$	05-09-1997
20402-01-16-00*	$\chi$	22-02-1997
20402-01-05-00	$\chi$	04-12-1996

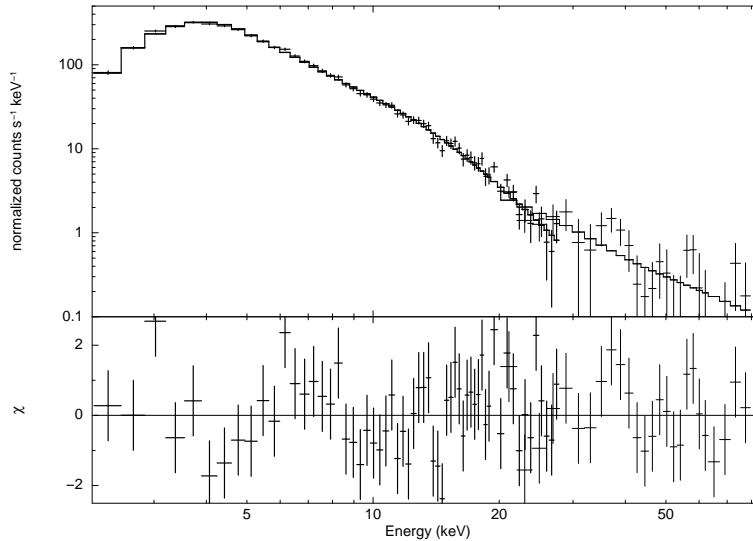


**Fig 1:** A sample spectrum with the fitted *diskbb* and power law components. The HEXTE data is also added.

Gaussian for iron line as required for best fitting. During fitting of the spectra we have adopted the technique taken by Sobczak et al. (1999), to obtain the values of spectral parameters. We have calculated error-bars at 90% confidence level in each case. In soft states, the *diskbb* model is fitted in the 2.0– $\sim$ 10.0 keV range. and in hard states the *diskbb* is fitted in the 2.0– $\sim$ 5.0 keV. This upper limit changes dynamically while fitting of the spectra.

To have the spectral evolution with time for each classes, we have generated PCA spectrum (2 to 40keV) with a minimum of 16s time interval along with the background spectrum and response matrix. This procedure is repeated with every 16s shift in time interval since the minimum time resolution in ‘standard2’ data is 16s. We use ‘timetrans’ task to select each and every step of time interval.

4 Partha Sarathi Pal, Sandip K. Chakrabarti, Anuj Nandi

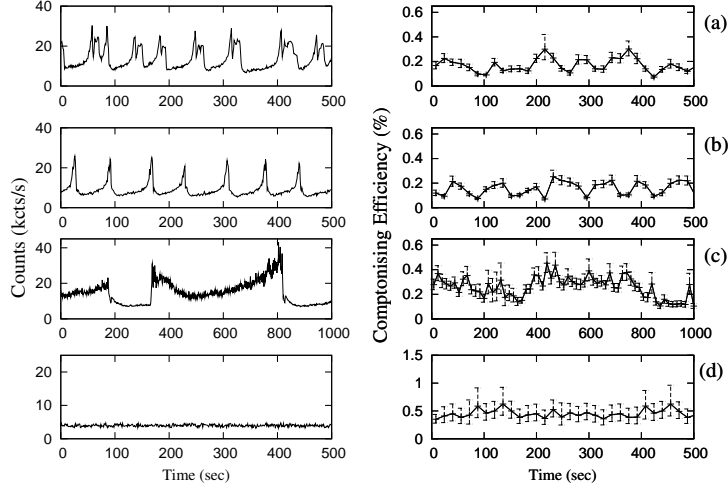


**Fig 2:** Results of the analysis of (a)  $\kappa$ , (b)  $\rho$ , (c)  $\theta$  and (d)  $\chi$  classes are shown. Left panel: Light curve in 2.0 – 40.0 keV range. Right panel: Comptonizing Efficiency (CE) in percent, obtained from 16s binned data.

### 3. The Efficiency of Comptonization

We first corrected for the (energy dependent) hydrogen column absorption feature because we are interested in the number photons which were originally emitted. We compute the photon numbers emitted in the power-law ( $N_{PL}$ ) and the multi-color blackbody components ( $N_{BB}$ ) and the ratio  $N_{PL}/N_{BB}$  will be called the Comptonization efficiency (CE). The number of black body photons are obtained following Makishima et al., (1986) and Comptonized photons  $N_{PL}$  are calculated by using the power-law equation given below,

$$P(E) = N(E)^{-\alpha}, \quad (1)$$

where,  $\alpha$  is the power-law index and  $N$  is the total counts/s/keV at 1keV. It is reported in Titarchuk (1994), that the Comptonization spectrum will have a peak around  $3 \times T_{in}$ . Thus the power law equation is integrated from  $3 \times T_{in}$  to 40keV to calculate total number of Comptonized photons in counts/s. The presence of line emissions are taken care of by usual Gaussian fits. Apart from the disk blackbody and power-law model, we also tried using CompST model (Sunyaev & Titarchuk, 1980). However, our conclusion remains the same. In the Fig. 1, we show an example of the fitted PCA spectrum with *diskbb* model along with the fitted components. We also show the residuals to characterize the goodness of the fit. Here we included HXETE data. However, in the rest we do not use HXETE data as the CE is not affected by more than a percent. The photon numbers and CE are calculated with the parameters obtained from the fitting. The black body spectrum is simulated with  $T_{in} = 1.15^{+0.057}_{-0.052}$  keV. The calculated number of black body photons from

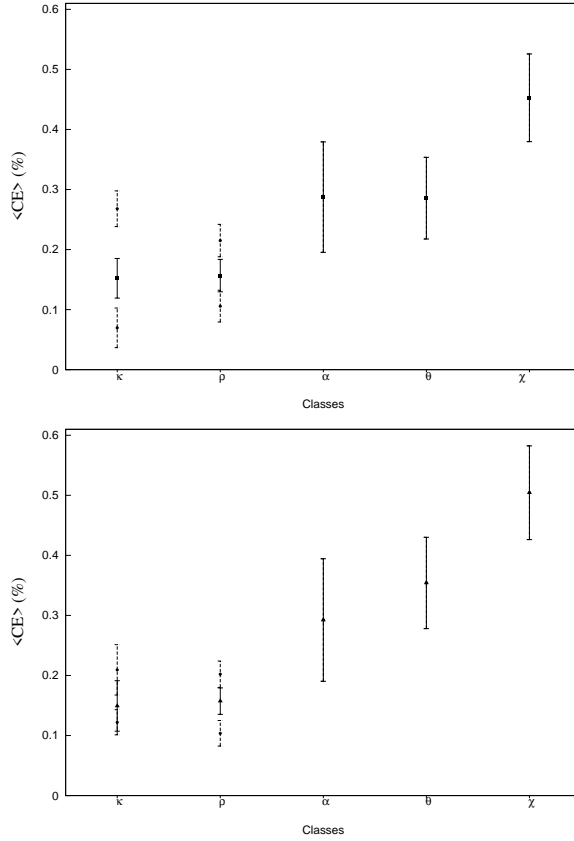


**Fig 3** Variation of averaged Comptonizing efficiency ( $\langle CE \rangle$ ). Average values of the two sets are shown in filled squares and filled triangles, while the average CE for a the burst-off and burst-on states of a given class is shown in filled circles. Note that all burst-off states have higher average CE values, while all burst-on states have lower average CE values indicating that the Compton cloud is of larger size.

0.1 – 6.5keV is  $156.03^{+17.10}_{-13.90}$  kcounts/s. In the same way, the power-law spectrum is simulated with the power-law index =  $2.057^{+0.154}_{-0.147}$ .

The calculated number of the Comptonized photons between 3.45 – 40 keV is  $0.39^{+0.06}_{-0.05}$  kcounts/s. The ratio between the power-law photon and the black body photon is  $0.25^{+0.08}_{-0.07}\%$ . This means that only 0.41% of the soft photons are Comptonized by the low angular momentum flow component generally referred to as the Centrifugal Pressure supported Boundary Layer or CENBOL.

In Table. 2, a comparison of the fitted parameters are given with error at 90% confidence level. The first column gives the class name and the second column gives the burst-off (hard) and the burst-on (soft) states, if present, in each class. The third column gives the black body temperature of the fitted Keplerian disk ( $T_{in}$  in keV). The fourth column gives the maximum energy in keV up to which *diskbb*

6 Partha Sarathi Pal, Sandip K. Chakrabarti, Anuj Nandi

model is fitted and soft photon number is calculated. The fifth column gives the count rates of the soft photons. The next column gives the index associated with the fitted power-law component. The seventh column gives the derived hard photon counts per second. The eighth column gives the ratio of the photon numbers of the fifth and the seventh columns. This is the so-called Comptonizing efficiency or CE. We arranged the classes in a way that the average CE changes monotonically. We find it to be high in harder classes and low in the softer classes. The final column gives the value of reduced  $\chi^2$  for the fits.

Class		$T_{in}$ (keV)	Energy keV	Soft Photon (kcnt/s)	Power law index	Hard Photon (kcnt/s)	CE (%)	$\chi^2$
$\kappa$	h	1.150 <sup>+0.057</sup> <sub>-0.052</sub>	6.5	156.03 <sup>+17.10</sup> <sub>-13.90</sub>	2.057 <sup>+0.154</sup> <sub>-0.147</sub>	0.39 <sup>+0.06</sup> <sub>-0.05</sub>	0.25 <sup>+0.08</sup> <sub>-0.07</sub>	1.2
	s	1.900 <sup>+0.027</sup> <sub>-0.026</sub>	8.0	432.72 <sup>+13.95</sup> <sub>-13.15</sub>	2.983 <sup>+0.243</sup> <sub>-0.234</sub>	0.21 <sup>+0.03</sup> <sub>-0.03</sub>	0.05 <sup>+0.010</sup> <sub>-0.008</sub>	1.5
$\rho$	h	1.382 <sup>+0.031</sup> <sub>-0.029</sub>	5.75	382.33 <sup>+18.42</sup> <sub>-16.73</sub>	2.505 <sup>+0.101</sup> <sub>-0.099</sub>	0.95 <sup>+0.09</sup> <sub>-0.08</sub>	0.25 <sup>+0.04</sup> <sub>-0.03</sub>	1.54
	s	1.843 <sup>+0.022</sup> <sub>-0.022</sub>	8.0	419.92 <sup>+11.55</sup> <sub>-10.97</sub>	2.331 <sup>+0.160</sup> <sub>-0.155</sub>	0.34 <sup>+0.04</sup> <sub>-0.03</sub>	0.08 <sup>+0.01</sup> <sub>-0.01</sub>	0.99
$\alpha$	-	1.213 <sup>+0.082</sup> <sub>-0.070</sub>	4.5	261.36 <sup>+38.46</sup> <sub>-28.74</sub>	2.067 <sup>+0.062</sup> <sub>-0.061</sub>	0.81 <sup>+0.04</sup> <sub>-0.04</sub>	0.31 <sup>+0.08</sup> <sub>-0.07</sub>	1.01
$\theta$	h	1.391 <sup>+0.039</sup> <sub>-0.037</sub>	6.0	416.84 <sup>+25.73</sup> <sub>-22.85</sub>	2.501 <sup>+0.089</sup> <sub>-0.087</sub>	1.15 <sup>+0.09</sup> <sub>-0.08</sub>	0.28 <sup>+0.05</sup> <sub>-0.04</sub>	1.3
	s	1.317 <sup>+0.034</sup> <sub>-0.032</sub>	5.5	388.95 <sup>+21.46</sup> <sub>-19.19</sub>	3.248 <sup>+0.157</sup> <sub>-0.152</sub>	0.65 <sup>+0.08</sup> <sub>-0.07</sub>	0.17 <sup>+0.03</sup> <sub>-0.03</sub>	1.5
$\chi$	-	1.200 <sup>+0.117</sup> <sub>-0.094</sub>	4.5	126.80 <sup>+27.74</sup> <sub>-18.46</sub>	1.968 <sup>+0.076</sup> <sub>-0.074</sub>	0.57 <sup>+0.03</sup> <sub>-0.03</sub>	0.45 <sup>+0.17</sup> <sub>-0.12</sub>	1.2

#### 4. Results

So far, we have shown that our model independent CE varies from one variability class to another. We now present the dynamical analysis of the light curves of some of the variability classes. In Figs. 2(a-d), we show the results of  $\kappa$ ,  $\rho$ ,  $\theta$  and  $\chi$  respectively. In each class we show two panels. The left panel is the variation of the photon counts with time and the right panel shows the variation of Comptonizing Efficiency (CE) calculated using 16 seconds of binned data. The error bar is provided at 90% confidence level. In Fig. 2a, an analysis of a 500s chunk of the  $\kappa$  class of observation is shown. The photon counts become high  $\sim 30,000/\text{sec}$  and low ( $\sim 10,000/\text{sec}$ ) aperiodically at an interval of about 50 – 75s. In the low count regions, the spectrum is harder and the object is in the burst-off state. The Keplerian photon varies between 150 to 450 kcounts/sec and Comptonized photon varies between 0.39 to 0.21 kcounts/sec. The average CE factor can vary from  $\sim 0.07$  to  $\sim 0.25$  depending on whether we have burst-on or burst-off respectively. In Fig. 2b, the blackbody photon count in the simulated spectrum varies between 350 to 420 kcounts/s and Comptonized photon counts vary around 0.95 to 0.34 kcounts/s. Hence CE rises to a maximum of 0.25%. In Fig. 2c, the analysis of a 1000s data of the  $\theta$  class is done. The  $\theta$  class can be divided in two regions depending on the photon count rates. In the soft dip region, the photon count is lower than 10000

counts/sec. In this region, the spectrum is softer and the CE amount of interaction is around 0.17%. In the other (hard dip) region, say between 350s and 820s, the photon count is higher and vary from 10,000 counts/sec to 30,000 counts/sec. In this region, CE reaches to a high value of 0.28%. It is believed that the CENBOL is suddenly removed by magnetic effects and the soft dip is formed (Nandi et al. 2001). In Fig. 2d, we show the results of  $\chi$  class. We note that the average Comptonizing efficiency (CE) to be  $\sim 0.4 - 0.5\%$ , the highest of all the classes discussed so far. We also analyzed an intermediate class called  $\alpha$  (which is basically a combination of the  $\rho$  and  $\alpha$  classes mentioned above. We find the CE We analyse the data of 2000s as this class displays a long time variation. The CE varies between 0.05% to  $\sim 0.6\%$  with an average of 0.3%.

## 5. Class transition due to variation in Geometry?

In Fig. 3(a-b), we plot the average CEs of the five classes we analyzed in the previous section. If we arrange them in the sequence of increasing average CE, we note that the sequence becomes  $\kappa \rightarrow \rho \rightarrow \alpha \rightarrow \theta \rightarrow \chi$ . We took two observations in each case and plotted both the cases, one with squares (a) and the other with triangles (b). A further division in average CE when both the burst-on and burst-off regions are present, is also shown with filled circles, the bottom one being for burst-on and the top one is for burst-off. In Papers I and II, examples were presented of  $\kappa \rightarrow \rho$ ,  $\chi \rightarrow \rho$ ,  $\chi \rightarrow \theta$ ,  $\rho \rightarrow \alpha$  transitions. In Naik et al. (2002b), where IXAE data was analyzed, the transitions  $\rho \rightarrow \alpha \rightarrow \chi$  were hinted at. We note that these transitions are expected:  $\kappa$  and  $\rho$  are adjacent;  $\chi$  and  $\theta$  are adjacent;  $\rho$  can transit to  $\chi$  via  $\alpha$ . The class  $\theta$  is an anomalous case as it is basically formed when the Compton cloud (in our picture, CENBOL) of a  $\chi$  class is abruptly removed. Similarly,  $\alpha$  is a combination of  $\rho$  and  $\chi$ . We thus have a natural explanation of the observed transitions in terms of the smooth variation of the average Comptonizing efficiency, which in turn depend of the geometry of the Compton cloud. Since  $\theta$  is an anomalous class which forms in presence of strong magnetic field only, it may be skipped in some transition. However, we claim that  $\kappa$  cannot transit to  $\chi$  directly, for instance, without passing through  $\rho$ .

## 6. Conclusion

In this paper, we have analysed the classes of GRS 1915+105 which have demonstrated class transitions. Purely in a model independent way, we computed the ratios of the power-law photons and the soft photons coming from the Keplerian disk in all these classes. We ignore very high energy photons from HXETE since its contribution is less than a percent and excluding this does not change our conclusion. Since the power-law photons are believed to be formed due to inverse Comptonization of the injected soft photons, the only way the ratio can change is to change the geometry of the Compton cloud. In CT95 model, the puffed-up

8 Partha Sarathi Pal, Sandip K. Chakrabarti, Anuj Nandi

part of the low angular momentum flow (CENBOL) remains big in harder (burst-off) states and collapses in softer (burst-on) states. Thus we naturally see that the average Comptonizing efficiency in burst-off states is higher than that in burst-on states. Not only that, all the observed transitions are found to reside side-by-side in the class vs. CE plane. In other words, for a transition, the average CE changes smoothly. This implies that the geometry of the Compton cloud also varies from class to class. The geometry of a Compton cloud can depend on several physical conditions. In CT95, the CENBOL collapses when the accretion rate of the Keplerian disk is increased. This in softer state, CE is low. When the disk rate is very low, the CENBOL cannot be cooled down. It remains big, as in an ion-pressure supported torus (Rees et al. 1982), and thus the interception of soft photons could be large, thereby increasing CE. We believe that this interpretation can be used even for classes not discussed in this paper. This work is being done and the results would be presented shortly.

Recently, Remillard and McClintock. (2006) presented evidences that perhaps GRS 1915+105 is an extremely rotating Kerr black hole. However, results discussed in this paper are directly the analysis of the observational data and the interpretation of variation of the Comptonizing efficiency is totally model independent. In other words, our conclusion of the variation of the geometry from one class to another remains valid even when the spin of the black hole is extreme.

The work of P. S. Pal is supported by CSIR fellowship.

## References

1. M. A. Abramowicz, W. Kluzniak, 2001, *Astron. Astrophys.* 374, L19
2. O.M. Blaes, E. Sramkova, M.A. Abramowicz, W. Kluzniak & U. Torkelson, 2007, *Astrophys. J.* 665, 653
3. S. K. Chakrabarti & A. Nandi 2000, *Ind. J. Phys.*, 75B(1), 1
4. S. K. Chakrabarti, A. Nandi, A. K. Chatterjee, A. K. Choudhury, & U. Chatterjee, 2005, *Astron. Astrophys.*, 431, 825
5. S. K. Chakrabarti, A. Nandi, A. K. Choudhury & U. Chatterjee, 2004, *Astrophys. J.*, 607, 406
6. S. K. Chakrabarti & L. G. Titarchuk, 1995, *Astrophys. J.* 455, 623 (CT95)
7. E. T. Harlaftis & J. Greiner, 2004, *Astron. Astrophys.* 414, L13
8. F. Haardt & L. Maraschi, 1993, *Astrophys. J.* 413, 507
9. S. Kato, 2008, *Publ. Astrophys. Soc. Japan*, 60, 111
10. Y. Kobayashi, A. Kubota, K. Nakazawa, T. Takahashi & K. Makishima 2003, *Pub. Astron. Soc. J.* 55, 273
11. K. Makishima et. al. 1986, *Astrophys. J.* 308, 635
12. M. P. Muno, E. H. Morgan & R. A. Remillard, 1999, *Astrophys. J.* 527, 321
13. S. Naik, A. R. Rao & S. K. Chakrabarti 2002a, *J. Astron. Astrophys.* 23, 213
14. S. Naik, P. C. Agrawal, A. R. Rao & B. Paul, 2002b, *Mon. Not. R. Astron. Soc.* 330, 487
15. A. Nandi, S. G. Manickam & S. K. Chakrabarti, 2001, *Mon. Not. R. Astron. Soc.* 324, 267
16. A. Nandi, S. K. Chakrabarti, S. V. Vadawale & A. R. Rao, 2001, *Astron. Astrophys.* 380, 245.

17. A. R. Rao, J. S. Yadav & B. Paul, 2000, *Astrophys. J.*, 544, 443
18. M. J. Rees, M. C. Begelman, R.D. Blandford & E. S. Phinney, 1982, *Nature* 295, 17
19. R. A. Remillard & J. E. McClintock, 2006, *Ann. Rev. Astron. Astrophys.* 44, 49
20. G. J. Sobczak, J. E. McClintock & R. A. Remillard et al. 1999, *Astrophys. J.* 520, 776
21. L. Stella & M. Vietri, 1999, *Phys. Rev. Lett.* 82, 17
22. T. E. Strohmayer, 2001 *Astrophys. J.* 554, 169
23. Z. Stuchlik, P. Slan, G. Trk, 2007, *Astron. Astrophys.* 470, 401
24. R. A. Sunyaev, & L. G. Titarchuk, 1980, *Astrophys. J.* 86, 121
25. L. G. Titarchuk, 1994, *Astrophys. J.* 434, 313
26. R. V. Wagoner, A. S. Silbergleit, M. Ortega-Rodriguez, 2001, *Astrophys. J.* 559, 25
27. J. S. Yadav, et al., 1999, *Astrophys. J.* 517, 935